WIRELESS WATER QUALITY MONITORING IN THE ISM FREQUENCY BAND: A SOFTWARE AND COGNITIVE RADIO APPROACH

A. Millot[1,3], *R. Feliachi*[3], *R. Weber*[2,3], *C. Léger*[3]

[1] ATCOM Telemetrie
15 rue jean Bertin, BP 79, 45430 Checy, France
phone: +33 2 38 46 63 00, fax: +33 2 38 86 28 91, email: millot@atcom.fr

[2] Observatoire de Paris
Station de radioastronomie, F-18330 Nançay, France
phone: +33 2 48 51 82 41, fax: +33 2 48 51 83 18 , email:rodolphe.weber@univ-orleans.fr

[3] Institut PRISME, Université d'Orléans
Site Galilée, 12 rue de Blois, 45067 Orléans cedex 2, France
phone: +33 2 38 49 45 62, email:christophe.leger@univ-orleans.fr

ABSTRACT

A long-range transmission demonstrator for low data rate environmental sensor networks is under development. It uses the ISM free-access frequency band at 433 MHz. In addition to distance attenuation, a major issue is the presence of numerous radio frequency interferences in this band. With a view to optimizing the sensor life and cost, the system complexity has been shifted to the central station which will be based on array processing techniques. In this paper, we describe a spatial cyclostationary detector for triggering the acquisition of sensor data frames in this highly corruptive radio environment.

1. INTRODUCTION

In recent years, water monitoring has become a great concern for all environmental decision-makers. However, classical off-line water monitoring (i.e. manual sampling or data loggers requiring manual downloading) are no longer suitable for current applications since it would be cost-prohibitive to collect data. Besides, new environmental regulations have defined more stringent requirements in term of efficiency, quality and costs. Among the monitoring alternatives, Wireless Sensor Networks (WSN) are very promising approaches[1]. For example, in [2], a fresh water monitoring system is described. The WSN is implemented through proprietary wireless networks, and secondary data transmission services (GSM or GPRS) provided by a mobile telephone operator. It is also possible to use free access bands. This is the case in [3] where a WSN based on IEEE 802.15.4 radio components at 2.4 GHz is used for precision agriculture or in [4] where a Berkeley Mica 2 Mote with a specific transceiver for low frequency transmissions (40 MHz) has been experimented. In both cases, the WSNs were designed to be used in open spaces with little human activity. In particular, no or few radio frequency interferences (RFI) occur during transmissions.

In this paper, the concept of a wireless water quality monitoring system in a highly corruptive radio environment is described. It is based on a low-rate one-way data stream over the 433 MHz ISM band. This free access band is widely used for remote control and the amount of RFI is very high. Moreover, power transmission is limited to 10 mW in this band. The challenge is to achieve long range transmission for our low data rate sensor array despite the presence of numerous RFI. To achieve low-cost and autonomous power objectives, the system complexity has been shifted to the reception level where a multi-antenna reception system will allow spatial signal processing. Since the transmission will be based on periodic (daily) short bursts of data, an off-line processing receiver is considered. In particular, demodulation and WSN data analysis will be done off-line.

In figure 1 the principles of our WSN are described. Detailed information is also available in [5]. In quiet radio environments, our prototype achieves a sensitivity which allows a long transmission range ($\gg$ 10 km). Thus, in this paper we focus on the RFI issue. In section 2, analyses of some recent RFI surveys in the 433 MHZ band are presented. Based on that knowledge, we propose to implement a spatial cyclostationary detector to trigger the automatic storage of the WSN waveforms. Section 3 describes this cyclostationary approach. In particular, the performances of several implementations are compared through simulations. In section 4, we conclude with some perspectives.

2. RFI ANALYSIS IN THE 433 MHZ ISM BAND

An experimental set-up has been developed for RFI surveys. It is based on a digital board from Xilinx (Xtreme DSP IV) which acquires the signal from a dedicated RF front-end centered in the 433 MHz ISM band. A digital down-converter is implemented in this board so that 10 kHz bandwidth waveforms can be acquired and stored in a computer for off-line statistical analysis. Several RFI survey campaigns have been conducted in a semi-urban area, for different frequencies and schedules. Figure 1.c shows the implantation of this receiver in suburb of Orléans (France). The location of the experimental relay station is also given for information. Figure 1.b compares the level of the relay station signal with the level of surrounding RFIs.

We have developed a dedicated software which al-

 ISSN 2076-1465

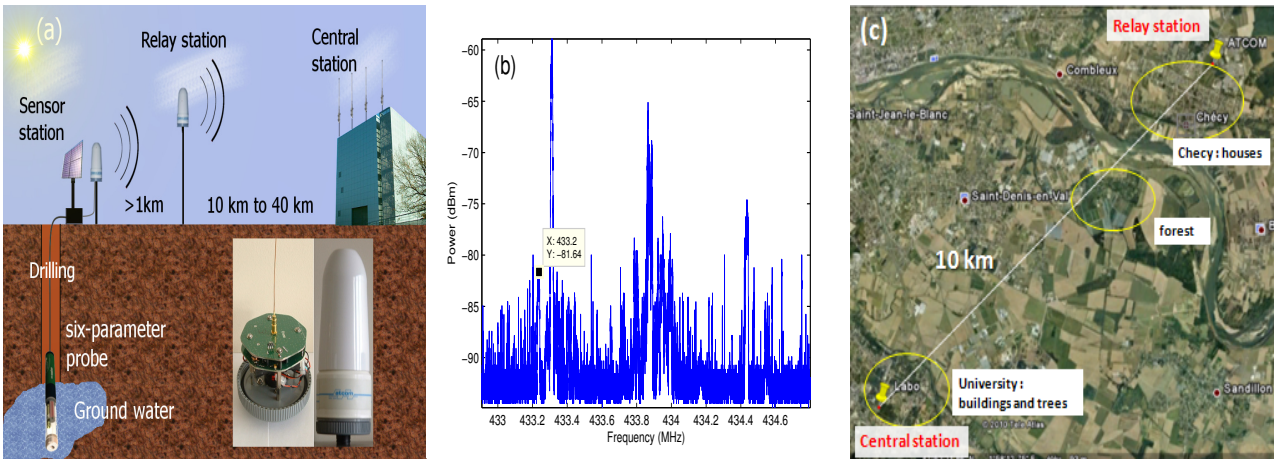

Figure 1: (a) Description of our wireless water monitoring network demonstrator. A six-parameter probe (Aqua50 from NeoTex-Ponsel) is buried in ground water. It communicates to a surface emitter through an SDI12 wire protocol. Within a radius of 1km, several ($\simeq$ 20) probe/emitter couples transmit their data to a relay station (pictures on the bottom right). Finally, all the relay nodes transmit probe information to a central receiver. This is a one-way star topology. The transmission is based on periodic (daily) short bursts of data (a few seconds at 1200 bds). In quiet radio environments, our prototype achieves a sensitivity which allows a long transmission range ($\gg$ 10 km). The main issue is the RFI present in the 433 MHz band. (b) Spectrum of the 433 MHz ISM band. It shows the maximum power over frequencies after 80 minutes of observation. The small black box corresponds to the received power level of our 10 mW relay station signal located 10 km away. Other spectral lines correspond to RFI. (c) Experiment location in the suburb of Orléans (France).

lows the automatic extraction of time and frequency RFI characteristics (bandwidth, duration, average power, peak power). The algorithm is based on iterative segmentation on power time-frequency planes derived from the data sets. Figure 2 gives an example of this automatic segmentation. The detection threshold was set to 3 times the system noise variance.

Table 1 provides some parameters extracted from some of these RFI survey campaigns. The first conclusion that can be drawn is that a better RFI environment can be found when transmitting during the night and aside from the ISM center frequency (i.e. f_0 =433.92 MHz). The main reason is that most remote devices transmit at 433.92 MHz and that human activity is obviously higher during the day. In the low occupancy 10 kHz band, we can consider that there is at most 1 RFI at a given instant. Another point is that 98% of the RFIs are shorter than 1 s with a bandwidth less than a few kHz.

3. CYCLOSTATIONARY DETECTION IN THE PRESENCE OF INTERFERENCE

Our relay station frames are short, typically less than a few seconds and there are only a few transmissions per day. To enhance the transmission performance in the presence of RFI, spatial filtering will be considered in a forthcoming evolution of the prototype. However, to limit both the hardware and the firmware costs, the objective is to accomplish it off-line. So, by considering the central station as a phased array, the first step is to trigger the acquisition of the array output vector at the right moment. Obviously, this can be done by scheduling the transmissions but we would also like to consider the case of emergency transmissions.

n°, when	f_0 (MHz)	RFI per hour	$\triangle T$ (s)	$\triangle F$ (kHz)
1, day	433.92	5277	0.3	1.6
2, night	433.92	4549	0.36	1.58
3, day	434.2	2864	0.28	1.31
4, night	434.2	567	0.32	1.33

Table 1: Average RFI characteristics from 4 RFI survey campaigns. f_0 is the center frequency of the 10 kHz bandwidth. For each f_0, night and day measurements have been conducted to observe the effect of human activity. *RFI per hour* corresponds to the average number of RFI detected per hour. $\triangle T$ and $\triangle F$ correspond respectively to the RFI average duration and bandwidth.

In this section, we propose an automatic triggering system based on the cyclic correlation matrices of the phased array. In subsection 3.1, we will define our array model. Then, in subsection 3.2, the cyclostationary approach will be described and finally in subsection 3.3, performances will be analyzed through simulations. In particular, a comparison with a classical power approach will be proposed.

3.1 Model description

Consider a phased array consisting of M antennas, each having a received signal $z_k(t)$, $k = 1, \cdots M$. From the previous discussions, it is clear that the narrow-band condition holds and that geometric delays for each antenna and each impinging source can be represented by phase shifts. In this case, the central station output vector can be modeled in complex base-band form as:

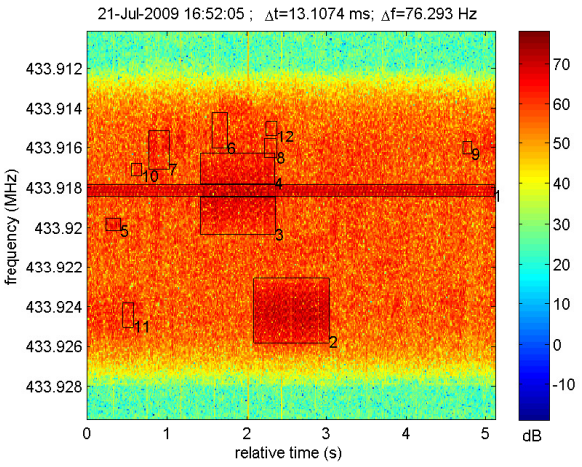

Figure 2: RFI analysis in the 433 MHz ISM band. The antenna signal is acquired with the Xilinx board and then, digitally down-converted to a 10 kHz bandwidth complex waveform (here, from 433.910 MHz to 433.920 MHz). Off-line, a filter bank with 256 channels provides a time-frequency representation for automatic segmentation. In the above example, 11 RFIs were detected (black boxes with a number on the bottom right). Box n°1 is a narrow band RFI, the others are impulsive RFIs.

$$\mathbf{z}(t) = \mathbf{a}_s s(t) + \mathbf{A}_r \mathbf{r}(t) + \mathbf{n}(t) \quad (1)$$

where:

- $\mathbf{z}(t) = [z_1(t)...z_M(t)]^T$ is the $M \times 1$ vector of central station signals at time t.
- $\mathbf{a}_s = [a_{1,s}...a_{M,s}]^T$ is the spatial signature of the relay station signal, $s(t)$.
- $\mathbf{r}(t) = [r_1(t)...r_K(t)]^T$ is the $K \times 1$ vector of the K interferers and $\mathbf{A}_r = [\mathbf{a}_{r_1}, \mathbf{a}_{r_2}, ..., \mathbf{a}_{r_K}]$ is a $M \times K$ matrix where each $\mathbf{a}_{r_k} = [a_{1,r_k}...a_{M,r_k}]^T$ is the spatial signature of the corresponding k^{th} RFI.
- $\mathbf{n}(t)$ is the system noise vector with independent Gaussian entries. There is no specific assumption made concerning the whitening of the covariance matrix and calibration of the data (i.e. $\left\langle \mathbf{n}(t)\mathbf{n}^{\mathbf{H}}(t) \right\rangle_\infty \neq \sigma^2\mathbf{I}$, where$\langle . \rangle_\infty$is the average operator and $\mathbf{I}$ is the $M \times M$ identity matrix).

At this stage, the phased array is not calibrated. Thus, all spatial signatures are modeled as random phase vectors.

3.2 Cyclostationary approach

Most telecommunication signals present a hidden periodicity due to the periodic characteristics involved in the signals construction (carrier frequency, baud rate, coding scheme...). These parameters are usually scrambled and hidden by the randomness of the message to be transmitted. However, by using a cyclostationary approach, this hidden periodicity can be recovered thus making identification of the telecommunications signal possible. An exhaustive overview of cyclostationarity theory and applications can found in [6, 7]. For array signal processing, cyclostationarity was introduced by Gardner [8]. In his analysis, the correlation matrix, $\mathbf{R}_\mathbf{z}(\tau) = \left\langle \mathbf{z}(t+\frac{\tau}{2})\mathbf{z}^{\mathbf{H}}(t-\frac{\tau}{2}) \right\rangle_\infty$, is replaced either by the cyclic correlation matrix:

$$\mathbf{R}_\mathbf{z}^\alpha(\tau) = \left\langle \mathbf{z}(t+\frac{\tau}{2})\mathbf{z}^{\mathbf{H}}(t-\frac{\tau}{2}) \exp(-j2\pi\alpha t) \right\rangle_\infty \quad (2)$$

or the cyclic conjugated correlation matrix:

$$\overline{\mathbf{R}}_\mathbf{z}^\alpha(\tau) = \left\langle \mathbf{z}(t+\frac{\tau}{2})\mathbf{z}^{\mathbf{T}}(t-\frac{\tau}{2}) \exp(-j2\pi\alpha t) \right\rangle_\infty \quad (3)$$

where α is the cyclic frequency. This parameter is linked to the above-mentioned periodic characteristics. Any signal with the right non-zero cyclic frequency will generate non-zero cyclic or cyclic conjugated correlation matrices. Inversely, any stationary signal or cyclostationary signal with different cyclic frequencies will generate zero in the above expressions. We will consider next that we do not receive cyclostationary interferences with the same cyclic frequencies as our WSN. Thus, the cyclic correlation matrix for our model defined by Eq. 1 becomes:

$$\mathbf{R}_\mathbf{z}^{\alpha_0}(\tau) = \mathbf{a}_s\mathbf{a}_s^H R_\mathbf{s}^{\alpha_0}(\tau) + \underbrace{\mathbf{A_r}\mathbf{R}_\mathbf{r}^{\alpha_0}(\tau)\mathbf{A}_\mathbf{r}^H}_{\to 0} + \underbrace{\mathbf{R}_\mathbf{n}^{\alpha_0}(\tau)}_{\to 0} \quad (4)$$

where α_0 is the WSN cyclic frequency and $R_\mathbf{s}^{\alpha_0}(\tau)$is the mono-dimensional version of Eq. 2. Similarly, the cyclic conjugated correlation matrix becomes:

$$\overline{\mathbf{R}}_z^{\overline{\alpha}_0}(\tau) = \mathbf{a}_r\mathbf{a}_r^T \overline{R}_\mathbf{s}^{\overline{\alpha}_0}(\tau) + \underbrace{\mathbf{A_r}\overline{\mathbf{R}}_\mathbf{r}^{\overline{\alpha}_0}(\tau)\mathbf{A}_\mathbf{r}^T}_{\to 0} + \underbrace{\overline{\mathbf{R}}_\mathbf{n}^{\overline{\alpha}_0}(\tau)}_{\to 0} \quad (5)$$

where $\overline{\alpha}_0$ is the WSN cyclic conjugated frequency and $\overline{R}_\mathbf{s}^{\overline{\alpha}_0}(\tau)$is the mono-dimensional version of Eq. 3.

In our application, the transmission between relay stations and the central station is based on a BPSK modulation scheme with a baud rate, $\frac{1}{T_0}$, and a carrier frequency, f_0:

$$s(t) = \exp(j2\pi f_0 t + j\varphi_0).\sum_{k\epsilon\mathbb{Z}} c_k h(t - kT_0 - t_0)$$

where c_k is the binary random sequence ($\left\langle |c_k|^2 \right\rangle_\infty = \sigma_c^2$), t_0 and φ_0 are unknown synchronization parameters and $h(t)$ is the pulse shaping function.

From [9], the expression of $R_\mathbf{s}^{\alpha_0}$and $\overline{R}_\mathbf{s}^{\overline{\alpha}_0}$can be derived:

$$R_\mathbf{s}^{\alpha_0}(\tau) = \frac{\sigma_c^2}{T_0}\exp(-j2\pi\alpha_0 t_0).\exp(j2\pi f_0\tau).r_h^{\alpha_0}(\tau)$$
$$\overline{R}_\mathbf{s}^{\overline{\alpha}_0}(\tau) = \frac{\sigma_c^2}{T_0}.\exp(-j2\pi(\overline{\alpha}_0 - 2f_0)t_0).\exp(j2\ell\varphi_0).r_h^{(\overline{\alpha}_0 - 2f_0)}(\tau)$$

where $\alpha_0 = \frac{k}{T_0}\ k\epsilon\mathbb{Z}^\star$, $\overline{\alpha}_0 = 2f_0 + \frac{k}{T_0}\ k\epsilon\mathbb{Z}$ and $r_h^\alpha(\tau)$ is given by:

$$r_h^{\alpha}(\tau) = \int_{-\infty}^{+\infty} h(t+\frac{\tau}{2})h(t-\frac{\tau}{2})\exp(-j2\pi\alpha t)dt$$

Except for a rectangular shaping function, $\exists k \neq 0$, $r_h^{\frac{k}{T_0}}(\tau = 0) \neq 0$. Thus, we will only consider next the case $\tau = 0$.

For the detection of our WSN signal, we propose to use the cyclic correlation matrix $\mathbf{R}_{\mathbf{z}}^{\alpha_0}$at $\alpha_0 = \frac{1}{T_0}$ or the cyclic conjugated correlation matrix $\overline{\mathbf{R}}_{\mathbf{z}}^{\overline{\alpha}_0}$ at $\overline{\alpha}_0 = 2f_0$. Equations 4 and 5 have shown that asymptotically these matrices depend on the WSN signal only. Therefore, these matrices are rank one and asymptotically, all their singular values are zeros except one. This maximum singular value is directly linked with $R_{\mathbf{s}}^{\alpha_0}$and $\overline{R}_{\mathbf{s}}^{\overline{\alpha}_0}$. We propose to test 3 detectors based on $\mathbf{R}_{\mathbf{z}}^{\alpha_0}$or $\overline{\mathbf{R}}_{\mathbf{z}}^{\overline{\alpha}_0}$:

- $T_\lambda(\mathbf{z})$ computes the maximum singular value of $\mathbf{R}_z^{\alpha_0}$or $\overline{\mathbf{R}}_z^{\overline{\alpha}_0}$
- $T_F(\mathbf{z})$ computes the Frobenius norm of $\mathbf{R}_z^{\alpha_0}$or $\overline{\mathbf{R}}_z^{\overline{\alpha}_0}$. The Frobenius norm is computationally less costly ($\mathcal{O}(M^2)$) than the singular value decomposition ($\mathcal{O}(M^3)$).
- $T_{diag}(\mathbf{z})$ computes the Frobenius norm of the diagonal of $\mathbf{R}_z^{\alpha_0}$or $\overline{\mathbf{R}}_z^{\overline{\alpha}_0}$. This is our very low computation complexity approach ($\mathcal{O}(M)$).

In the following section, the performances of the different cyclic detection algorithms will be studied, and compared to classic detectors based on $\mathbf{R}_\mathbf{z}$. In particular, the different correlation matrices will be estimated over a finite set of samples ($\langle . \rangle_\infty \Rightarrow \langle . \rangle_N = \frac{1}{N}\sum_N(.)$).

3.3 Performance analysis

For the simulations, the following signal model is considered:

$$\begin{array}{ll} H_0: & \mathbf{z}(t) = \sqrt{\rho}\mathbf{a}_r r(t) + \sqrt{1-\rho}\mathbf{n}(t) \\ H_1: & \mathbf{z}(t) = \sigma_s \mathbf{a}_s s(t) + \sqrt{\rho}\mathbf{a}_r r(t) + \sqrt{1-\rho}\mathbf{n}(t) \end{array}$$

The spatial signatures $\mathbf{a}_s$and $\mathbf{a}_r$ are chosen randomly ($\|\mathbf{a}_s\| = \|\mathbf{a}_r\| = 1$ and $M = 8$), $s(t)$ is BPSK signal with $f_0 = 0.1$, $T_0 = 8$, $h(t)$ is a root-raised cosine filter (50 coefficients, roll-off factor=0.5). The RFI, $r(t)$, is also BPSK modulated but with $f_1 = 0.318$, $T_0 = 13$. The system noise, $\mathbf{n}(t)$, is assumed to be independent Gaussian entries. The interference to noise ratio is defined by $INR = \frac{\rho}{1-\rho}$ with $0 \leq \rho < 1$. The signal to noise plus interference ratio is defined by $SNR = \sigma_s^2$.

Monte Carlo simulations are performed on different reception scenarios. The Fisher criterion is used to evaluate the performances of the detectors:

$$Fisher = \frac{\left(E_{H_1}\left[T_k(z)\right] - E_{H_0}\left[T_k(z)\right]\right)^2}{var_{H_1}(T_k(z)) + var_{H_0}(T_k(z))} \; k = \lambda,\, F,\, diag$$

where $E_{H_{0,1}}[.]$ and $var_{H_{0,1}}(.)$ are respectively the mean and the variance under the H_0 or H_1 hypothesis.

1. scenario 1: RFI is present and the noise is calibrated (i.e. $\left\langle \mathbf{n}(t)\mathbf{n}^{\mathbf{H}}(t)\right\rangle_\infty = \mathbf{I}$). Figure 3 draws the performances for different ρ and SNR. As expected, the sensitivity of the classic approach (based on $\mathbf{R}_\mathbf{z}$) can be clearly seen. Indeed, such power based detectors cannot distinguish between WSN and RFI signals. On the contrary, the cyclostationary approaches are very robust. For example, whatever the RFI level, the "cyclic $T_\lambda(\mathbf{z})$" behaves as a "classic $T_\lambda(\mathbf{z})$ with no RFI". Note that $T_F(z)$ detectors are less efficient than $T_\lambda(\mathbf{z})$ detectors. Indeed, cyclic correlation matrices are no longer rank one since they are estimated over a finite set of samples. Therefore the $M-1$ weaker singular values are no longer equal to zero. Since the $T_F(z)$ detector is the sum of the singular values, uncertainty is added.
2. scenario 2: no RFI but uncalibrated noise (i.e. $\left\langle \mathbf{n}(t)\mathbf{n}^{\mathbf{H}}(t)\right\rangle_\infty \neq \mathbf{I}$). Figure 4 draws the performances for different SNR and different percentages of noise fluctuations between antennas. Once again, the robustness of cyclostationary approaches can be observed.
3. scenario 3: a realistic simulation with 10% noise fluctuations and one RFI with $SNR = 8dB$. Figure 5 draws the performances for different INR and different numbers of samples. Better performances are obtained with $\overline{\alpha}_0 = 2f_0$ than with $\alpha_0 = \frac{1}{T_0}$. The reason is that $r_h^{(\overline{\alpha}_0 - 2f_0)} > r_h^{\alpha_0}$. However, in practice it could be difficult to have exact knowledge of f_0 before any carrier synchronization. Note that $T_{diag}(z)$ detectors are less efficient than $T_F(\mathbf{z})$ detectors. Indeed, less cyclic information is used in the second case. In fact, $T_{diag}(z)$ can be seen as the average of M mono-dimensional cyclostationary detectors. From these simulations and from measurements on site ($INR = -15dB$ and $SNR = 8dB$ at 40 km), to ensure correct detection (Fisher >10) of our WSN signal at 40 km, $N = 2048$ samples (respectively $N = 8192$) are necessary for $T_F(\mathbf{z})$ (resp. $T_{diag}(z)$) with $\alpha_0 = \frac{1}{T_0}$. These values go down to $N = 512$ with $\overline{\alpha}_0 = 2f_0$.

4. PERSPECTIVES

In the framework of wireless environmental monitoring, a radio frequency interference (RFI) survey has been conducted in the 433 MHz ISM free-access band. From analysis of the RFI characteristics, three new detectors based on cyclostationarity have been proposed. The objective is to detect the signal of interest (SOI) with a phased array in a highly corruptive environment. These algorithms have demonstrated by simulation their robustness against the presence of interferences or uncalibrated noise. These results are based on the fact that the cyclic correlation or cyclic conjugated correlation matrices depend asymptotically only on the SOI cyclostationary property. The next step will be to use one of these detectors to trigger the acquisition of SOI frames in real time. Then, triggered data are stored for off-line spatial filtering technique (MVDR), demodulation and analysis.

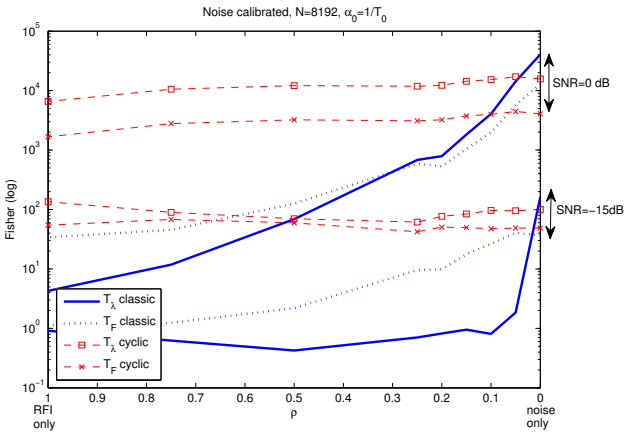

Figure 3: Detector performances for scenario 1. The RFI is present and the noise is calibrated (i.e. $\left\langle \mathbf{n}(t)\mathbf{n}^{\mathbf{H}}(t)\right\rangle_{\infty} = \mathbf{I}$). Correlation matrices are estimated with $N = 8192$ samples. The 2 sets of curves are associated respectively to the 2 SNR given on the right.

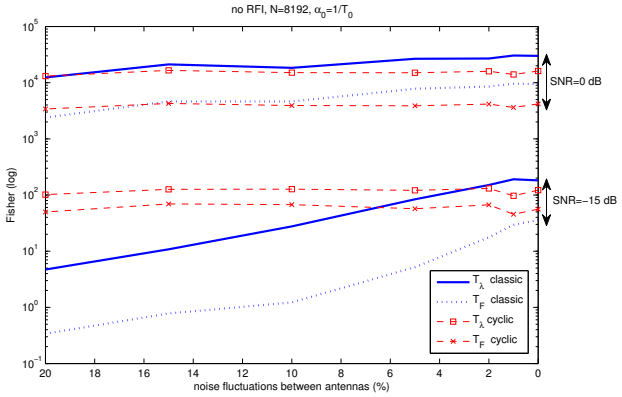

Figure 4: Detector performances for scenario 2. No RFI but noise is uncalibrated (i.e. $\left\langle \mathbf{n}(t)\mathbf{n}^{\mathbf{H}}(t)\right\rangle_{\infty} \neq \mathbf{I}$). Noise fluctuations vary from 0% to 20%. Correlation matrices are estimated with $N = 8192$ samples. The 2 sets of curves are associated respectively to the 2 SNR given on the right.

Acknowledgments

The authors would like to thank the Region Centre, the French agency ANRT, the French funding committee (FRED), the Ministère de la Recherche and the European committee (ERDF) for funding part of this work. This work was undertaken in collaboration with the Pôle Capteurs Automatismes de Bourges, France.

REFERENCES

[1] Jennifer Yick, Biswanath Mukherjee, and Dipak Ghosal. Wireless sensor network survey. *Computer Networks*, 52(12):2292–2330, August 2008.

[2] J.V. Capella, A. Bonastre, R. Ors, and M. Peris. A wireless sensor network approach for distributed in-line chemical analysis of water. *Talanta*, 80(5), 2010.

[3] J.A. López Riquelme, F. Soto, J. Suardíaz, P. Sánchez, A. Iborra, and J.A. Vera. Wireless sensor networks for precision horticulture in Southern Spain. *Computers and Electronics in Agriculture*, 68:25–35, August 2009.

[4] Simon Willis and Cornelis Jan Kikkert. Radio propagation model for long-range wireless sensor networks. In *2007 6th International Conference on Information, Communications & Signal Processing*, pages 1–5, Singapore, 2007.

[5] Anthony Millot, Rodolphe Weber, and Catherine Berho. Transmission de données environnementales en bande ISM. Application à la surveillance à distance des masses d'eau. *REE*, 11, 2009.

[6] Erchin Serpedin, Flaviu Panduru, Ilkay Sari, and Georgios B. Giannakis. Bibliography on cyclostationarity. *Signal Processing*, 85(12):2233–2303, December 2005.

[7] William A. Gardner, Antonio Napolitano, and Luigi Paura. Cyclostationarity: Half a century of research. *Signal Processing*, 86(4):639–697, April 2006.

[8] W.A. Gardner. Simplification of MUSIC and ESPRIT by exploitation of cyclostationarity. *Proceedings of the IEEE*, 76(7):845–847, 1988.

[9] W.A. Gardner. Exploitation of spectral redundancy in cyclostationary signals. *Signal Processing Magazine, IEEE*, 8(2):14–36, 1991.

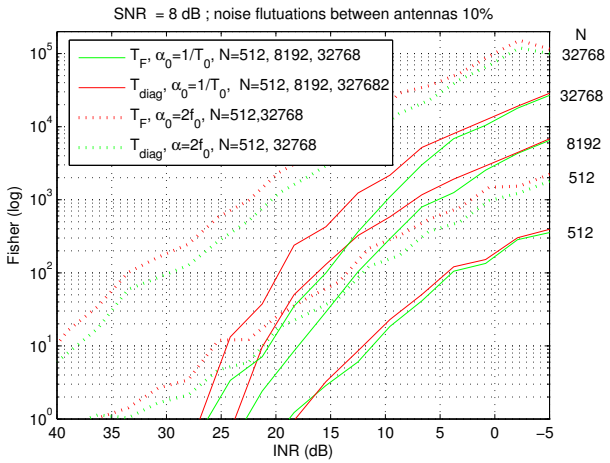

Figure 5: Cyclostationary detector performances for scenario 3. It corresponds to a realistic simulation with 10% noise fluctuations and one RFI with $SNR = 8\,dB$ (this value corresponds to a 40 km transmission). For continuous lines, $\mathbf{R}_z^{\alpha_0}$ with $\alpha_0 = \frac{1}{T_0}$ was used. For dashed lines, $\overline{\mathbf{R}}_z^{\overline{\alpha}_0}$ with $\overline{\alpha}_0 = 2f_0$ was used. Correlation matrices are estimated with N samples. The 5 sets of curves are associated respectively to the 5 values of N given on the right.